Effect of nitrogen post-doping on a commercial platinum–ruthenium/carbon anode catalyst

CrossMark

April R. Corpuz [a], Kevin N. Wood [b], Svitlana Pylypenko [b,*], Arrelaine A. Dameron [c],
Prabhuram Joghee [b], Tim S. Olson [c], Guido Bender [c], Huyen N. Dinh [c], Thomas Gennett [c],
Ryan M. Richards [a], Ryan O'Hayre [b]

[a] Department of Chemistry, Colorado School of Mines, 1500 Illinois Street, Golden, CO 80401, United States
[b] Department of Metallurgical and Materials Engineering, Colorado School of Mines, 1500 Illinois Street, Golden, CO 80401, United States
[c] National Renewable Energy Laboratory, 1617 Cole Boulevard, Golden, CO 80401, United States

HIGHLIGHTS

- Commercial carbon-supported PtRu catalyst is post-doped with nitrogen.
- Nitrogen post-doping improves initial performance by more than 16%.
- Nitrogen-doped catalyst retains ~34% more surface area than unmodified catalyst.
- MEA with N-modified PtRu/C retains performance while unmodified PtRu/C loses ~33%.
- Post-doping improves performance of the best performing commercial catalysts.

ARTICLE INFO

ABSTRACT

This work investigates the effects of after-the-fact chemical modification of a state-of-the-art commercial carbon-supported PtRu catalyst for direct methanol fuel cells (DMFCs). A commercial PtRu/C (JM HiSPEC-10000) catalyst is post-doped with nitrogen by ion-implantation, where "post-doped" denotes nitrogen doping after metal is carbon-supported. Composition and performance of the PtRu/C catalyst post-modified with nitrogen at several dosages are evaluated using X-ray photoelectron spectroscopy (XPS), rotating disk electrode (RDE), and membrane electrode assemblies (MEAs) for DMFC. Overall, implantation at high dosage results in 16% higher electrochemical surface area and enhances performance, specifically in the mass transfer region. Rotating disk electrode (RDE) results show that after 5000 cycles of accelerated durability testing to high potential, the modified catalyst retains 34% more electrochemical surface area (ECSA) than the unmodified catalyst. The benefits of nitrogen post-doping are further substantiated by DMFC durability studies (carried out for 425 h), where the MEA with the modified catalyst exhibits higher surface area and performance stability in comparison to the MEA with unmodified catalyst. These results demonstrate that post-doping of nitrogen in a commercial PtRu/C catalyst is an effective approach, capable of improving the performance of available best-in-class commercial catalysts.

1. Introduction

Recent advancements in electrocatalysis and improvements in fuel cell components are bringing polymer electrolyte membrane fuel cells (PEMFCs) closer to commercial viability. However, further improvements in fuel cell durability, particularly through the mitigation of electrocatalyst degradation, are needed [1,2]. As a result, there is an increasing research activity aimed at developing a fundamental understanding of and improving catalyst utilization and stability. Among a variety of strategies for improving catalyst

* Corresponding author. Tel.: +1 303 273 3106; fax: +1 303 273 3795.
  E-mail addresses: april.corpuz@gmail.com (A.R. Corpuz), kewood@mymail.mines.edu (K.N. Wood), spylypen@mines.edu, Svitlana.Pylypenko@nrel.gov (S. Pylypenko), Arrelaine.Dameron@nrel.gov (A.A. Dameron), pjoghee@mines.edu (P. Joghee), Guido.Bender@nrel.gov (G. Bender), Huyen.Dinh@nrel.gov (H.N. Dinh), Thomas.Gennett@nrel.gov (T. Gennett), rrichard@mines.edu (R.M. Richards), rohayre@mines.edu (R. O'Hayre).

performance, efforts focusing on modifying carbon support chemistries and optimizing low temperature catalyst–support interactions have recently led to significant improvements [3–5].

The genesis of interest in modified carbon support materials for PEMFCs and DMFCs originated in the mid-1990s, when it was hypothesized that changing the chemical structure of carbon through functionalization could lead to potential catalyst stability benefits due to tailored catalyst–support interactions [4]. Today, researchers have shown that a variety of heteroatoms, such as nitrogen [5–17], boron [15,16], phosphorus [16], sulfur [17], iodine [18], and fluorine [18] can effectively change the physical, chemical and electronic properties of carbon-based catalyst support materials in ways beneficial to their performance. Among many doping approaches, ion implantation shows particular promise as it is a scalable, semiconductor industry-adopted process that has been shown to be an effective route to incorporate dopants into carbon-based materials, including high-surface area supports [7,9,11,14,19].

The most widely studied heteroatom modifier is nitrogen because of its abundance, accessibility, low health risk, and promising results [7,20–23]. Noble-metal nanoparticle catalysts supported on nitrogen-modified carbon-based materials, when compared against unmodified supports, have shown improved dispersion, durability and catalytic activity for a variety of fuel-cell relevant electrochemical reactions, including the hydrogen oxidation reaction, the methanol oxidation reaction, and the oxygen reduction reaction [17,24–31]. More recently, theoretical DFT work and experimental studies conducted on model supports (highly oriented pyrolytic graphite; HOPG) have provided additional insight into the effect of nitrogen on nanoparticle catalyst durability [32–34]. These studies have identified the importance of nitrogen concentration and nitrogen defect clustering on overlying catalyst nanoparticle activity and durability. Typically, nitrogen-containing supports are not limited to one specific nitrogen functional group, but rather contain a wide spectrum of species, including nitrogen in graphitic, pyridinic, pyrrolic, and quaternary forms, as well as multi-nitrogen defects. Identifying which specific nitrogen groups are responsible for the observed enhancement in binding between catalyst and support is still a focus of considerable discussion. DFT analysis suggests that the effect of nitrogen on Pt and PtRu stability can be either beneficial or detrimental depending on the specific nitrogen functionality introduced into the carbon support, and for maximum beneficial effects it appears necessary to have a balance of graphitic, pyridinic and pyrrolic functionalities [33].

Continued understanding of these materials has also been provided by energy electron loss (EEL) spectral imaging, which has revealed a spatial correlation between the most stable nanoparticles and higher amounts of nitrogen in the carbon support [33,34]. Studies suggest that this correlation is likely due to both a reduction in nanoparticle dissolution and a reduction in nanoparticle agglomeration/coarsening facilitated by the dopant [23,26].

In our recent work, we have transitioned from the evaluation of model and high-surface area materials in half-cell configurations to membrane electrode assembly (MEA) single-cell fuel cell studies [35,36]. It has been demonstrated that a DMFC MEA employing an N-doped PtRu/C anode retained more electrochemically active anode surface area and sustained only half as much ruthenium cross-over as an MEA employing an otherwise identically synthesized undoped PtRu/C anode [36]. The DMFC performance of N-doped PtRu/C MEA was likewise better sustained compared to the undoped PtRu/C MEA after durability testing (5× higher current density at 0.4 V after 625 h durability testing). Materials evaluated in these previous studies were doped with nitrogen prior to metal deposition. Therefore, the nitrogen dopants could be distributed throughout carbon surface, both underneath and between the subsequently deposited catalyst nanoparticles.

The current work further examines the effects of nitrogen modification by studying the performance of a pre-existing state-of-the-art commercial catalyst implanted with nitrogen. In this case, nitrogen doping (via nitrogen ion implantation) is conducted on a commercial 60 wt% PtRu/C catalyst, consisting of PtRu nanoparticles already deposited onto a high surface area carbon support. Due to the shadowing effect caused by the pre-existence of the PtRu nanoparticles during the N-implantation process, the nitrogen heteroatom incorporation is expected only in regions of the carbon structure unshielded by PtRu nanoparticles. This work therefore helps to further advance fundamental understanding of the way in which nitrogen improves the stability of the nanoparticle catalysts while exploring a facile pathway for the enhancement of current industry leading products.

To assess the effects of post-doping on state-of-the-art carbon supported PtRu catalysts, unmodified and post-modified samples were characterized and compared using both RDE experiments and MEA tests. These studies demonstrate that after durability testing, the post-modified state-of-the-art commercial catalysts outperform the unmodified benchmark catalyst.

2. Experimental

2.1. Materials

The commercial anode catalyst used in these studies is nominally 60 wt% PtRu supported on carbon black (Johnson Matthey HiSpec® 10000). Specifically, the platinum weight loading is 39.39% and the ruthenium weight loading is 18.91%, as given by the company specifications for the specific lot used.

For the modification of samples with nitrogen, approximately 500 mg of PtRu/C catalyst was placed into a rotating sample holder (rotating wheel), and the chamber was evacuated to less than 5×10^{-6} Torr [37,38]. Prior to nitrogen ion implantation, powders were out-gassed by heating to above 180 °C for 15 min. Samples were then implanted with a 3 cm DC ion source (Veeco) at a pressure of 1×10^{-3} Torr (N$_2$) at two different dosages by changing the beam current between 12 mA and 45 mA, while maintaining a constant discharge voltage (55 V) and acceleration voltage (100 V) for 60 min.

2.2. Characterization

Thermogravimetric analysis (TGA) was done using the TA Q600 (TA Instruments, New Castle, DE) by feeding 100 mL min^{-1} of synthetic air (80% N$_2$, 20% O$_2$) with a heating rate of 5 °C min^{-1} to a temperature of 850 °C. The total metal content of the catalyst powders was determined based on the assumption that the final mass at 850 °C is composed of RuO$_2$ and Pt. The Transmission Electron Microscopy (TEM) micrographs of undoped and post-modified PtRu/carbon were obtained on a Philips CM200 TEM. In addition to initial evaluation of catalyst powders, samples were also collected from the anode surface of the cycled MEA's.

XPS analysis was performed on a Kratos Nova X-ray photoelectron spectrometer using pass energies of 160 eV for the survey spectra and 20 eV for the high-resolution spectra of C 1s/Ru 3d, O1s, N1s, Ru 3p, and Pt 4f. Data processing was carried out using Casa XPS software and involved background subtraction, charge calibration, and curve fitting. A linear background was applied to O 1s and N 1s regions, while Shirley background was used for C1s/Ru3d, Pt4f and Ru3p regions. Charge referencing was done to the carbon peak at 284.8 eV. Consistent fitting parameters and constraints were applied to the C1s/Ru 3d region to obtain the distribution of

ruthenium species. The Ru 3d region was fitted with 4 peaks, each containing 3d$_{5/2}$ and 3d$_{3/2}$ components separated by 4.2 eV, as shown in Fig. 1 and Table 1. Elemental quantification of ruthenium was performed using the Ru 3p region.

2.3. RDE studies

Initial electrochemical studies of post-modified PtRu/C catalyst powders included rotating disk electrode (RDE), cyclic voltammetry (CV), and CO stripping voltammetry. Electrochemical measurements were conducted at room temperature in a standard three-electrode configuration that utilized a saturated calomel reference electrode (SCE), a Pt mesh counter electrode and a thin-film layer of the catalyst (applied from an ink) as the working electrode. RDE electrodes were prepared using 1 mg mL^{-1} solutions of catalyst inks made with 10 mg of the catalyst powder, 7.96 mL of water, 2 mL of 2-propanol (IPA), and 40 μL of 5 wt% Nafion solution. These mixtures were bath sonicated for 20 min and 10 μL of the ink was then applied to the glassy carbon RDE tip. The electrodes were then dried at 40 °C for 30 min. Prior to performing CO stripping voltammetry, the working electrode was electrochemically cleaned in a solution of 1 M H$_2$SO$_4$ by cycling 5 times from 0.05 to 0.80 V versus RHE. Then, pure CO gas was bubbled into 1 M H$_2$SO$_4$ for

10 min while the working electrode was held at 0.1 V versus RHE. While the working electrode was still held at 0.1 V versus RHE, pure N$_2$ was bubbled for 10 min to purge excess CO from the electrolyte. The potential was then swept to 0.9 V versus RHE at 20 mV s^{-1} to strip the adsorbed CO from the surface of the working electrode. Two subsequent sweeps from 0 to 0.9 V were then performed to ensure that all the bulk CO had indeed been removed from the electrode.

2.4. MEA fabrication

Two MEAs with a geometric area of 5 cm^2 each were fabricated for single-cell fuel cell studies. The anode ink was made by mixing 40 mg of anode catalyst (either the unmodified commercial PtRu/C or the PtRu/C post-modified with nitrogen at beam current 45 mA, PtRu/C–N2) with 320 mg 5 wt% Nafion in alcohol and 300 mg water. Subsequently, the anode ink was then hand-painted onto a Nafion 117 membrane over a vacuum table at 70 °C using a 5 cm^2 mask. The catalytic ink painted on the membrane was dried over the vacuum table. Then, the anode-coated membrane was hot-pressed at 130 °C with 294 lbs for 10 min. The approximate catalyst (total metal) loading was maintained to 3 mg cm^{-2} for each anode. During MEA assembly into the fuel cell hardware, 5 cm^2 carbon paper with a microporous layer (SGL GDL 25BC) was placed on PtRu/carbon anode to facilitate fuel distribution to the anode. For the cathode side, a commercial Pt-coated (0.4 mg cm^{-2}) gas diffusion electrode (GDE), ELE062 (procured from Johnson Matthey), was placed directly opposite to the anode, with the Nafion 117 membrane sandwiched in-between the electrodes.

2.5. MEA testing

Before measuring the initial DMFC performance, the MEAs were broken-in [39–41] at 70 °C, using 1 M methanol at flow rate of 0.7 mL min^{-1} and 60 sccm air with 100% relative humidity and back-pressure of 3 psi. After allowing the open circuit voltage (OCV) to rise above 0.75 V, the fuel cell was set at 0.35 V for 10 min with a 3.3 stoichiometric air-flow. It was then subjected to a series of potential cycles. Each potential cycle began at 0.35 V for 30 min, after which the potential was increased in 0.05 V increments up to 0.7 V at 10 s intervals. This procedure was repeated for a total of six cycles. The cell was then brought to OCV and cooled to 50 °C with continuous reactant flow, followed by termination of the air-flow, then the methanol flow, in that order. The cell was then allowed to sit overnight at room temperature to continue hydration of the Nafion.

A variety of electrochemical tests (anode CO stripping, cathode CO stripping, methanol/H$_2$ polarization (also called methanol oxidation reaction, or MOR) on the anode, and methanol/air polarization) were conducted after break-in as well as intermittently during the long term performance durability testing. This durability test was carried out for both MEAs for 425 h. CO stripping was performed at 25 °C by flowing 300 sccm of 1% CO in Ar at 100% relative humidity (RH) for 30 min to the electrode of interest (either in the anode or in the cathode), followed by flowing 300 sccm 100% RH N$_2$ for 30 min. During that time, H$_2$ was flowed at 100 sccm and 100% RH on the other electrode, which thereby served as both a counter and pseudo reference-electrode (dynamic hydrogen electrode, DHE). In this paper the DHE does not refer to an external electrode with its own current, but simply refers to the cell being run in 'driven mode', where either the cathode or anode is flowed with humidified H$_2$ and serves as both a counter and reference-electrode [42]. CO stripping was carried out on the respective electrodes (either anode or cathode) by holding a constant potential of 0.1 V vs. DHE. Cyclic voltammetry (CV) was then performed
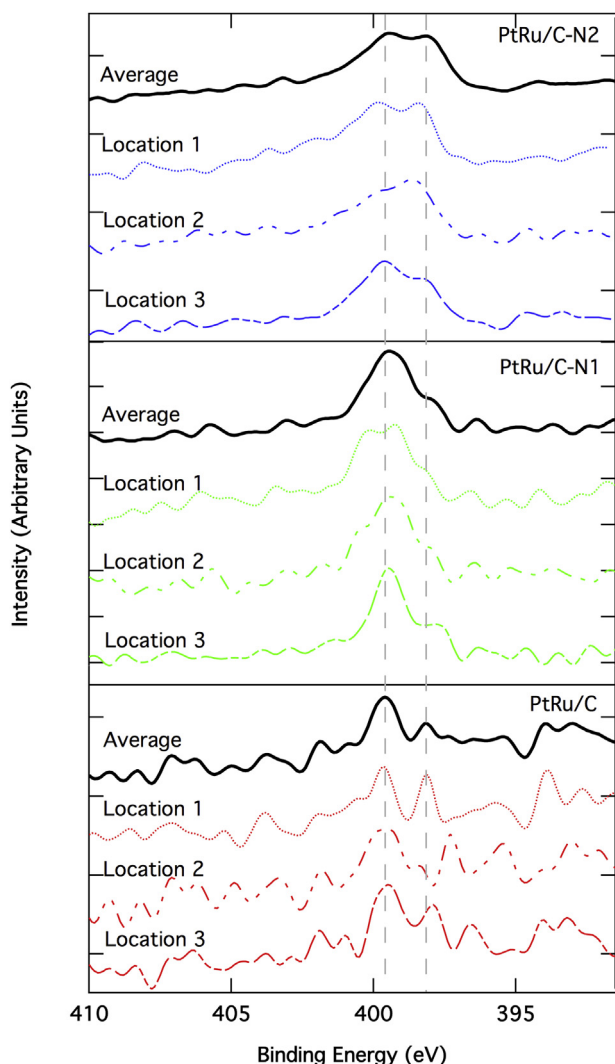

Fig. 1. High resolution N1s spectra, shown for three areas on each sample and their average.

Table 1
XPS analysis: elemental composition, and quantification of deconvoluted XPS spectra of Ru3d, and Pt 4f, reported as average of three areas per sample.

Sample	PtRu/C	PtRu/ C−N1	PtRu/ C−N2
Implantation beam current, mA	0	12	45
Elemental concentration, at%			
Carbon, C 1s	82.6	80.5	77.5
Oxygen, O 1s	10.1	10.8	11.4
Nitrogen, N 1s	0.2	1.1	1.7
Platinum, Pt 4f	3.3	3.7	4.5
Ruthenium, Ru 3p	3.8	3.9	4.9
Pt + Ru	7.2	7.6	9.3
Pt/Ru	1.1	1.1	1.1
Quantification of Ru3d, relative concentration, %			
Ru metallic: Ru1 (280.6 eV) and Ru5 (284.8 eV)	34.0	29.9	24.4
RuO_2, screened state: Ru2 (281.4 eV) and Ru6 (285.6 eV)	38.3	38.3	42.8
RuO_2*nH_2O (or RuO_xH_y): Ru3 (282.5 eV) and Ru7 (286.7 eV)	10.7	12.7	18.9
RuO_2, unscreened final state and/or RuO_3: Ru4 (283.7 eV) and Ru8 (287.9 eV)	17.1	19.1	13.9
Quantification of Pt 4f, relative concentration, %			
Pt metallic: Pt1 (72.2 eV) and Pt4 (75.5 eV)	53.1	51.6	48.6
Pt in oxide and hydroxide states: Pt2 (73.1 eV) and Pt5 (76.4 eV), and Pt2 (75.1 eV) and Pt5 (78.3 eV)	47.0	48.4	51.4

between 0.05 and 0.90 V vs. DHE for three cycles at a scan rate of 5 mV s^{-1}. During CV measurement, no gases were passed over the electrode of interest (either anode or cathode) while 50 sccm of 100% H_2 was fed to the opposite electrode (the DHE). MOR polarization curves were collected at 70 °C by flowing 1 mL min^{-1} of 1 M methanol on the anode and 50 sccm of 100% RH H_2 on the cathode. Again, the Pt cathode with H_2 flow was used as a counter and pseudo-reference electrode, i.e., as a DHE. A linear-sweep voltammogram was performed from 0 to 0.7 V vs. DHE at a scan rate of 2 mV s^{-1}. Data between 0.2 and 0.5 V was used. Methanol/air polarization curves were acquired by feeding 1 M methanol at a flow rate of 0.7 mL min^{-1} to the anode and 3.3 stoichiometric air flow (100% RH) to the cathode side (minimum flow of 60 sccm) at 80 °C. Constant current steps, 15 min in duration, were used to generate the polarization curve, with the last 5 min of data averaged to produce each voltage point for the polarization curve.

DMFC durability testing was carried out at 80 °C by feeding 1 M methanol at a flow rate of 0.7 mL min^{-1} to the anode and 3.3 stoichiometric oxidant flow of 100% RH air on the cathode side (minimum flow of 60 sccm). Each fuel cell was then held at 0.4 V for a total of 425 h. Durability testing was stopped intermittently for electrochemical testing.

3. Results and discussion

3.1. Material characterization

Table 1 summarizes changes to the elemental composition of the commercial PtRu/C catalyst after doping with nitrogen as a function of ion implantation conditions. XPS shows that nitrogen was successfully incorporated into the materials with concentration between 1 and 2 at.% as compared to levels of 3−5 at.% for the same implantation condition without metals [43]. Fig. 1 shows high-resolution N1s spectra for the catalyst powder samples as a function of implantation dosage, demonstrating that there is some variation within each sample, as evaluated by analyzing three areas per sample. The high level of noise in the N1s spectra obtained on PtRu/C−N1 is due to the presence of multiple functionalities (pyridinic, pyrrolic, amine, graphitic, amine, etc.) [10,12,14,27,35,44–48] spreading over a large range of binding energies (BE), with each being present in relatively small amounts. Increase in the implantation dosage resulted in an increase in the total amount of nitrogen, while still producing a wide spectrum. The shape of the nitrogen spectrum however appears to change with the increase in the nitrogen dosage indicating that the ratio of nitrogen species at lower binding energy (pyridinic, amine) to species at higher binding energy (graphitic, pyrrolic) is different. Specifically, higher implantation dosages appear to favor the formation of a greater percentage of lower-binding energy nitrogen species. In previous work with PtRu supported on pre-doped HOPG substrates, we have found correlation between the most improved stability and higher amounts of low binding energy species such as pyridinic nitrogen (albeit in the presence of other species such as pyrrolic and graphitic nitrogen) [26]. We hypothesize that the electronic effects of nitrogen post-doping are likely to be similar to those of nitrogen pre-doping, where higher amounts of lower binding energy species (corresponding to longer implantation times) may be more favorable for improving stability.

TGA analysis confirmed that materials before and after nitrogen implantation have the same metal loading, ∼60 wt%. Based on XPS analysis, the ratio of surface Pt to Ru was also maintained at 1:1 for all samples, but the total amount of surface Pt and Ru was changed from the original catalyst, especially for the sample modified at a higher dosage (PtRu/C−N2) (Table 1). In addition, ion implantation
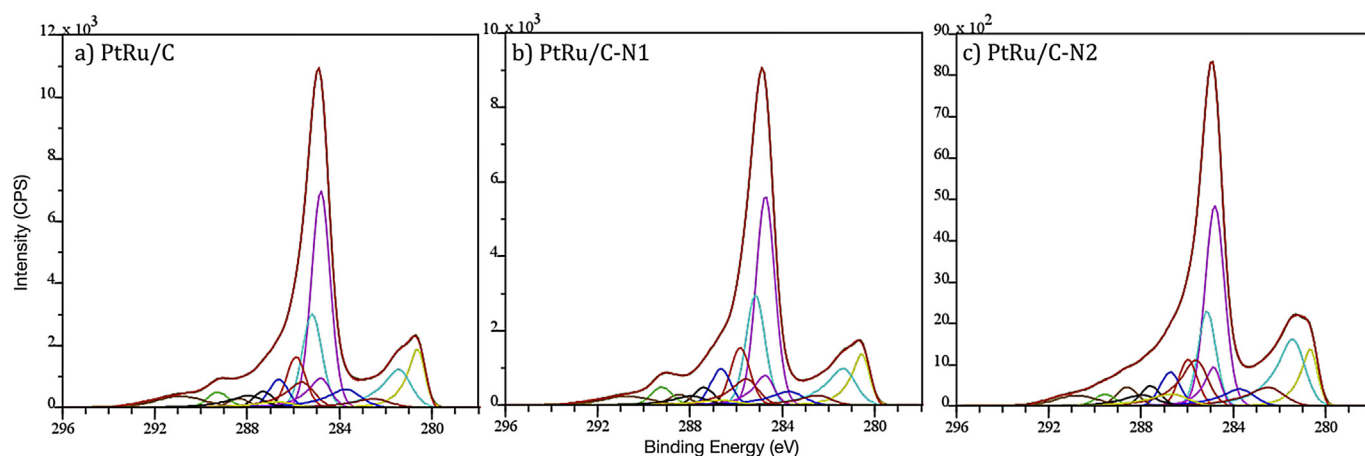

Fig. 2. High resolution C 1s + Ru 3d spectra, curve-fitted a) PtRu/C, b) PtRu/C−N1, and c) PtRu/C−N2.

also affected the distribution of the ruthenium and platinum species, decreasing the relative amount of metallic components and increasing the oxide components (Table 1 and Fig. 2).

TEM images in Fig. 3 shows three areas representative of the three different types of nanoparticle distribution and coverage, typical for 60 wt% PtRu/C before (Fig. 3, a1–a3) and after modification with nitrogen (Fig. 3, b1–b3). Analysis of these (unmodified and post-modified PtRu/C) images shows that a large fraction of catalyst is agglomerated, complicating analysis of individual nanoparticles (Fig. 3 a1 and b1). Fig. 3 a2 and b2 shows regions of carbon black with more disperse nanoparticles. Fig. 3 a3 demonstrates that regions with high metal coverage often neighbor regions with little to no metal on the carbon support. While images of PtRu/C–N2 in Fig. 3 b1 and b2 are similar to those found in undoped PtRu/C, areas such as shown in Fig. 3 b3 are only found in the post-doped materials (including materials post-modified at low implantation dosages). These regions have small PtRu nanoparticles evenly distributed on the surface of the carbon support and we hypothesize that their appearance results from ion-implantation-induced redistribution of the PtRu nanophase from regions with high metal coverage to regions with low metal coverage. Appearance of areas such as those shown in Fig. 3 b3 are expected to increase the relative concentration of platinum and ruthenium to carbon detected with XPS, consistent with our experimental data (Table 1). To summarize the findings from XPS and TEM, during ion implantation, particularly at a high dosage, a fraction of PtRu reorganizes on the surface of the carbon support to form small well-dispersed nanoparticles that are richer in hydrous and anhydrous oxides than the original catalyst.

3.2. RDE studies

Electrochemical surface area (ECSA) for the unmodified PtRu/C catalyst powder and post-modified PtRu/C catalyst powders was determined using standard CO stripping analysis (assuming a stripping charge of 420 μC cm^{-2}). Initial CO stripping curves obtained for the unmodified and post-modified materials (Fig. 4) indicate that the post-modified catalysts show a more positive "kick-off" potential for the removal and oxidation of the adsorbed CO as compared to the commercial unmodified benchmark. As mentioned before, while XPS shows that the platinum to ruthenium ratio (including both metallic and oxide species) stays the same for all samples, there are differences in the metallic and oxide species due to ion implantation. The PtRu phase in post-modified samples shows a somewhat higher concentration of ruthenium and platinum oxide species. XPS also shows that the post-doped materials are more deficient in metallic Ru components when compared to the unmodified material. This suggests that the shift in CO stripping onset potential might be related to redistribution of surface Pt and Ru species.

The material modified using a low implantation dosage (PtRu/C–N1) has a lower ECSA (39.1 m^2 g^{-1}) than the unmodified catalyst (56.3 m^2 g^{-1}). In contrast, the material modified using a high implantation dosage (PtRu/C–N2) exhibits a higher ECSA (65.2 m^2 g^{-1}) than the unmodified material. This is consistent with XPS results, which show the sample implanted at higher dosage has higher combined surface concentrations of Pt and Ru (Table 1). TEM observations also suggest that PtRu is reorganized on the surface in such a way that active PtRu surface area increases, as explained earlier. After initial surface area tests, each sample electrode was subjected to accelerated degradation testing (ADT) through potential cycling from 0 to 0.9 V vs. RHE. Detailed graphs showing the CO stripping curves as a function of cycles (measured after 0, 50, 100, 1000 and 5000 electrochemical potential cycles) are included in Fig. 4, while the resultant CO stripping areas are shown in Fig. 5. For all samples, upon initial cycling (after 50 and 100 cycles), the onset potential slightly shifted towards more negative values. Then after 1000 cycles onset potential significantly shifted towards more
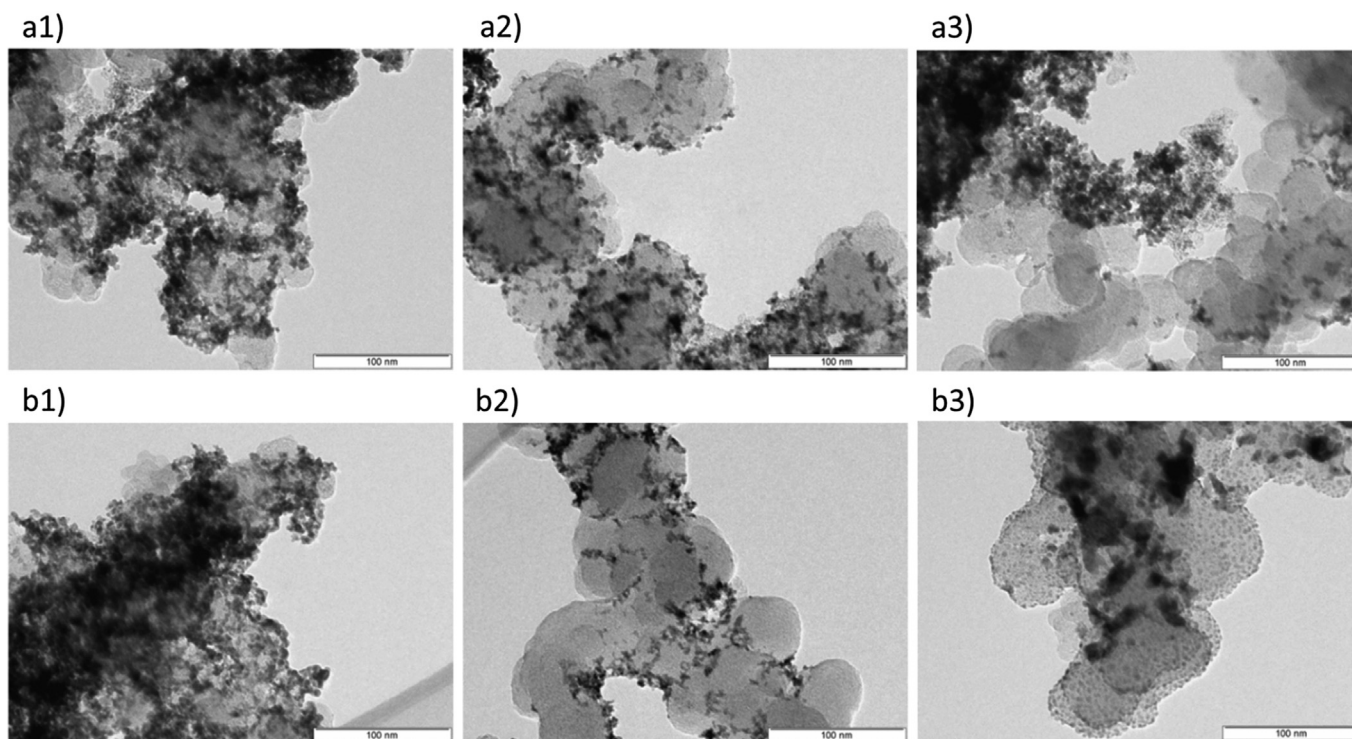

Fig. 3. TEM micrographs demonstrating three types of metal coverage for the catalysts a) PtRu/C, and b) PtRu/C–N2. b1 and b2 demonstrate morphology similar to the original catalyst. b3 shows areas with small well dispersed nanoparticles not observed in the original catalyst.
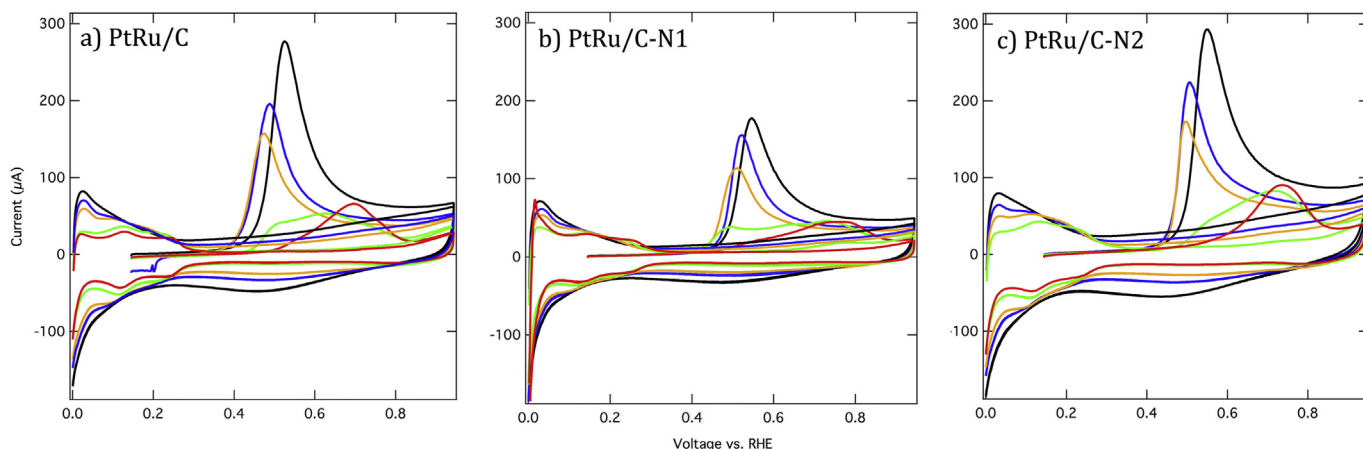
Fig. 4. CO stripping data of unmodified JM10000 and post-modified JM10000 catalysts as a function of cycling.

positive values (∼0.2 V), which was subsequently maintained through 5000 cycles. The initial and final (after 5000 cycles) curves of all samples are compared in Fig. S1 of the Supplementary information.

After 5000 cycles (Fig. 4), a significant decrease in current density is observed for every sample, and the peak positions shift toward more positive onset potentials (as described above, this shift appeared after 1000 cycles) indicating changes to the catalyst composition, possibly resulting from Pt enrichment originated from dissolution of ruthenium. Plotting the ECSA values for all samples as a function of cycling allows the beneficial effects of post-modification to be clearly observed (Fig. 5). Before cycling, the ECSA of PtRu/C–N2 was 16% higher than the unmodified PtRu/C. After each ADT segment the difference in ECSA between the two samples further widens, so that after 5000 cycles the PtRu/C–N2 sample maintains 34% higher ECSA than that of its unmodified counterpart.

It is interesting that despite differences in initial surface areas between unmodified PtRu/C and PtRu/C modified at low implantation dosages, their surface areas are almost identical after the first 1000 cycles and even after 5000 cycles. Meanwhile, PtRu/C modified at high implantation dosage starts with and, most importantly, maintains higher surface area throughout the entire cycling range.

In these experiments, it is difficult to conclusively show that improved durability results from nitrogen incorporation and not simply from changes to the PtRu phase, but it is highly suggestive that both of these factors impacted the performance. Reorganization of the PtRu phase becomes evident even at low dosages but does not result in better preservation of active surface area. Also, advantages of the implantation at higher dosages over low dosages and unmodified samples follow the trend observed in previous work, where samples were modified with nitrogen prior to metal deposition [23,26,35,36,38,49]. Based on work with model HOPG substrates, more aggressive dosages are expected to lead to the formation of multi-clustered nitrogen defects [26,27] that may act as effective trapping states to mitigate the migration of the catalyst nanoparticles.

3.3. MEA studies

In order to make comparisons under conditions closer to those used commercially, the post-doped material implanted at high implantation dosage (PtRu/C–N2) and the unmodified commercial catalyst were compared in MEA DMFC studies. An MEA made with a PtRu/C–N2 anode and a standard cathode (Pt/C GDE, 0.4 mg cm^{-2}) was compared to another MEA made with the
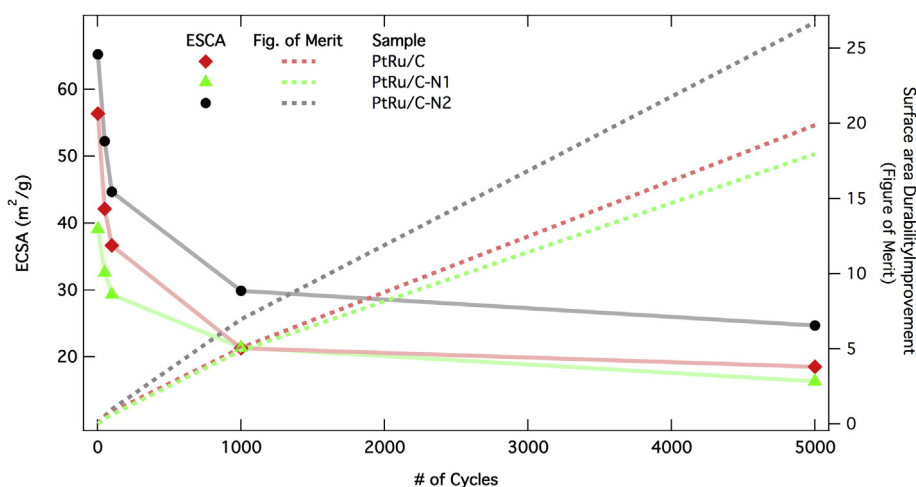

Fig. 5. The electrochemical surface area (ESCA) of unmodified JM10000 and post-modified JM10000 catalysts as a function of cycling. The electrochemical surface area is shown on the left axis. The right axis is a figure-of-merit plot where the surface area is multiplied by the percent of cycles completed during that testing segment (i.e. 52.2 × (50/5000) after 50 cycles and 24.7 × (4000/5000) after 5000 cycles) and then accumulated over the lifetime of the electrode.

unmodified PtRu/C and a standard cathode over the course of a long-term (425 h) durability test. The initial electrochemical characterization of the two MEAs is provided in Fig. 6. As shown by the anode CO stripping voltammograms in Fig. 6a, both anode catalysts show a narrow, single CO stripping peak, indicating a narrow distribution in the PtRu alloy [42]. The calculated electrochemical surface areas (ECSAs) from Fig. 6a are 0.58 m^2 and 0.75 m^2 for the PtRu/C and the PtRu/C−N2 anodes respectively, corresponding to 40 m^2 g^{-1} and 48 m^2 g^{-1} respectively when normalized by the metal mass-loadings of the two MEAs. This corresponds to about 20% increase in the ECSA for the nitrogen modified anode, a result which is well supported by RDE measurements of the catalyst powders that indicated about 16% increase in the ECSA for the PtRu/C−N2 powder relative to the unmodified control. The higher ECSA of the MEA anode employing the post-doped catalyst also correlates with the higher amount of surface platinum and ruthenium species detected with XPS (Table 1). These observations suggest that ion implantation results in the exposure of more surface Pt and Ru, likely due to reorganization of PtRu on the surface evident from TEM analysis. Similar to what was observed in the RDE experiments, PtRu/C has a slightly more negative CO oxidation onset peak than PtRu/C−N2; shown in Fig. 6a. Again, this can be explained by comparison to the XPS studies. Table 1 shows that PtRu/C−N2 has more Pt and Ru than PtRu/C, while maintaining an almost identical overall Pt:Ru ratio, however the ratio of metallic species (Pt and Ru) is not the same after post-doping. Table 1 also shows that PtRu/C−N2 is more
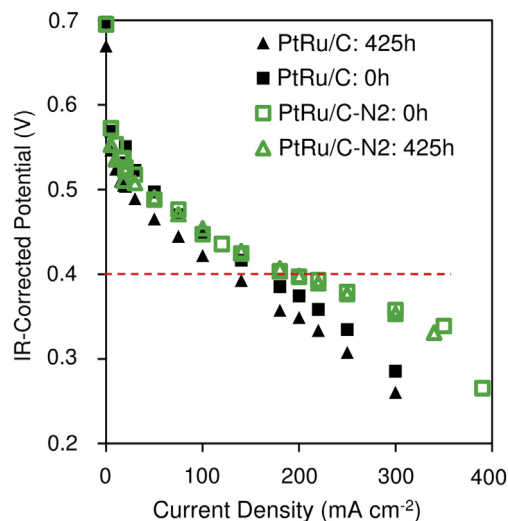

Fig. 7. DMFC performance curves before and after 425 h of durability. Data was taken at 80 °C with 0.7 mL min^{-1} of 1 M methanol flow on the anode side. Oxidant flow on the cathode side was 3 stoichiometric air flow with 60 sccm minimum flow.

deficient in its metallic ruthenium component than PtRu/C (and respectively more enriched in its metallic Pt component). Gasteiger et al. determined that a Pt:Ru ratio with 46% atomic Ru produces the lowest CO oxidation peak potentials in comparison to
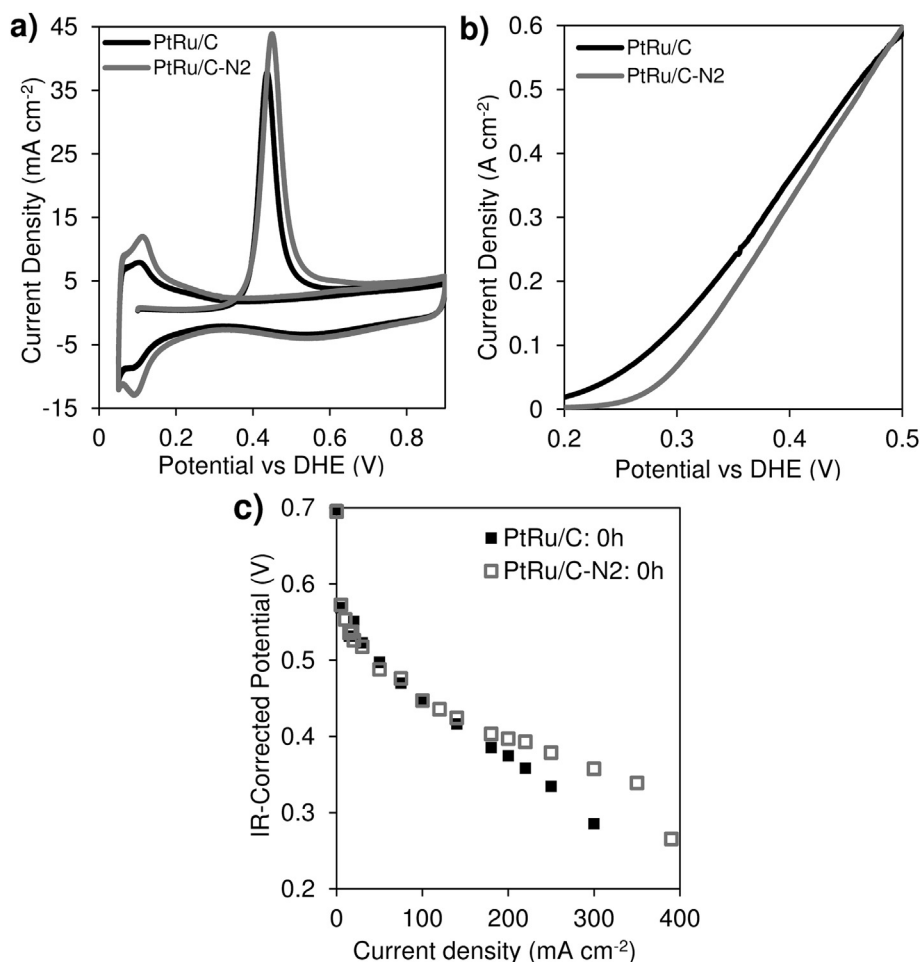

Fig. 6. Initial electrochemical characterization of the MEAs. a) Anode CO stripping curves, 5 mV s^{-1}, b) methanol oxidation reaction (MOR), 2 mV s^{-1}, c) methanol:air polarization curves, 80 °C.

other ratios, and predicted that a 1:1 Pt-to-Ru ratio would be the most favorable for CO oxidation [50].

As shown in Fig. 6b, both MEAs have comparable initial MOR performance at 0.4 V, with the MEA made with unmodified PtRu/C yielding 0.36 A cm^{-2}, and the MEA made with post-doped PtRu/C–N2 yielding 0.33 A cm^{-2}. However, the MEA made with PtRu/C–N2 shows a later onset in its MOR curve than the MEA made with PtRu/C. We attribute the later onset to the difference in Pt and Ru species between PtRu/C–N2 and PtRu/C, with PtRu/C–N2 having less ideal composition. As mentioned earlier, other studies on high-surface area PtRu catalysts have shown a 1:1 metallic Pt:Ru ratio to be the most favorable for methanol

electrooxidation [51–53], suggesting that the difference in onset in Fig. 6b may be because PtRu/C–N2 is somewhat deficient in metallic ruthenium component, as shown in Table 1. From Fig. 6c, both MEAs show similar initial direct methanol fuel cell (DMFC) performance. At 0.4 V, a standard operating voltage, the MEA made with PtRu/C–N2 generates approximately 190 mA cm^{-2}, and the MEA made with PtRu/C generates approximately 161 mA cm^{-2}. Also, the MEA made with PtRu/C–N2 performs slightly better in the mass-transport regime. This may be related to the higher ECSA of PtRu/C–N2, particularly if higher ECSA is due to better dispersions and higher accessibility of the active sites [54,55].
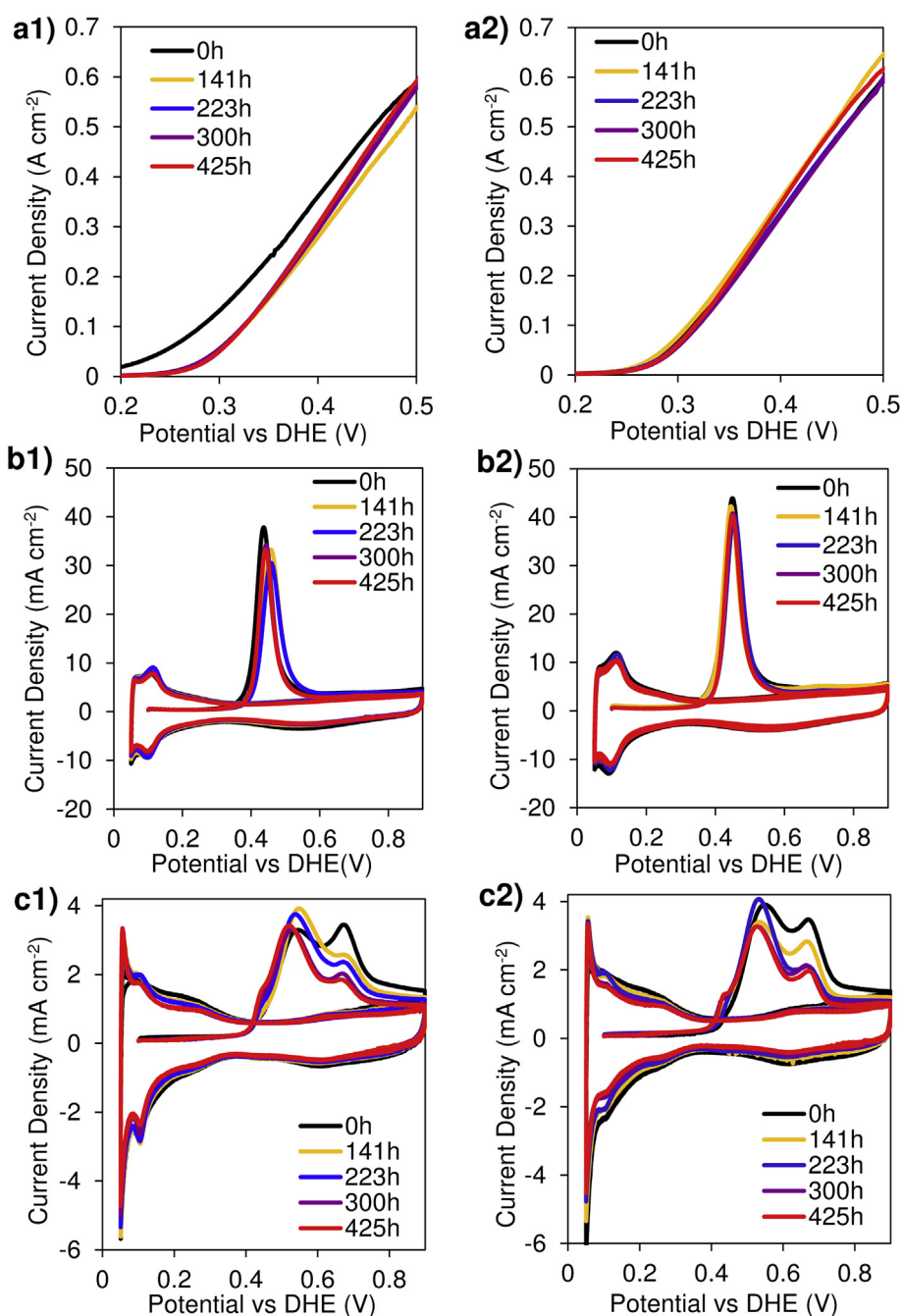

Fig. 8. a) Methanol oxidation reaction (MOR), b) anode CO stripping and c) cathode CO stripping as a function of durability testing time for the MEAs fabricated with the 1) unmodified PtRu/C anode and 2) PtRu/C–N2 anode respectively.
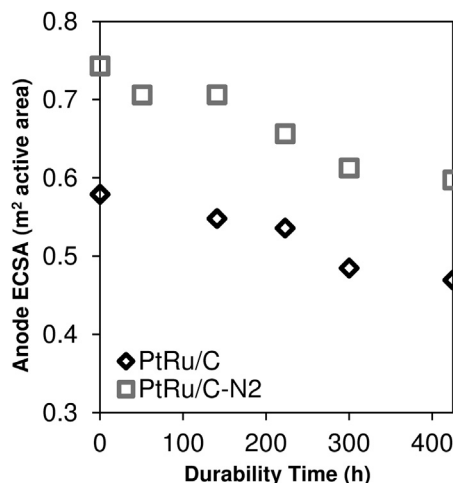
Fig. 9. Anode ECSA as measured from anode CO stripping at 5 mV s^{-1}.

Durability testing on the two MEAs was conducted by holding each fuel cell at 0.4 V under standard DMFC operating conditions (70 °C, 0.70 mL min^{-1} 1 M MeOH, 3.3 air stoichiometry at 100% RH). The two MEAs were each tested for 425 h of total durability time, with intermittent electrochemical measurements. Fig. 7 shows DMFC performance curves before and after the durability test period. After 425 h of durability testing, the MEA made with the undoped commercial anode shows an observable loss in performance across the entire operating range (e.g. ~33% loss in performance at 0.4 V). This is not the case for the MEA made with the post-doped anode catalyst, which fully retains its DMFC performance without any losses, thereby confirming the remarkable DMFC durability advantages provided by the nitrogen post-doping treatment.

The MOR data as a function of durability testing time for both MEAs is shown in Fig. 8a. From Fig. 8a, the MEA fabricated with the post-doped PtRu/C–N2 anode catalyst retains most of its anode performance (90% or greater) during the 425 h of durability testing. This is not the case with the undoped PtRu/C anode, which drops to 85% of its initial performance after durability testing when considering the current drawn at 0.4 V. Also, for the undoped PtRu/C, the onset potential shifts positively with operating time, suggesting changes in PtRu alloy ratio [53].

CO stripping on the anode as a function of durability for the two MEAs is shown in Fig. 8b. The potential of the CO stripping peak and the onset (Supplementary Fig. 3) for the unmodified PtRu/C anode shifts significantly during durability testing. It shifts positively after 141 and 223 h of durability testing, then negatively after 300 and 425 h of durability. These shifts are indicative of changes in catalyst composition, i.e. the ratio between platinum and ruthenium species [42]. The CO stripping peak of the PtRu/C–N2 anode shifts noticeably less during durability testing, which is evidence of a more stable catalyst. Both anodes exhibit narrow CO stripping peaks during durability testing, indicating a well-formed PtRu alloy. Also, after 425 h of durability testing, neither anode exhibits new peaks other than that of the PtRu alloy, indicating that there has been no formation of separate Pt or Ru phases [42]. Figs. 8b and 9 demonstrate that both anodes lose ECSA as a function of durability testing time. However, the nitrogen post-doped PtRu/C–N2 anode has higher ECSA than its unmodified counterpart (as measured by the area under the CO stripping curve) throughout durability testing. Remarkably, after 425 h of durability, ECSA of the post-doped PtRu/C–N2 is close to that of undoped PtRu/C before durability testing.

Fig. 8c shows CO stripping on the cathode as a function of durability testing time for the two MEAs. The peak around 0.70 V is assigned to pure Pt, and the peak at 0.55 V is assigned to pure Ru originating from Ru crossover [42]. While the cathodes of both
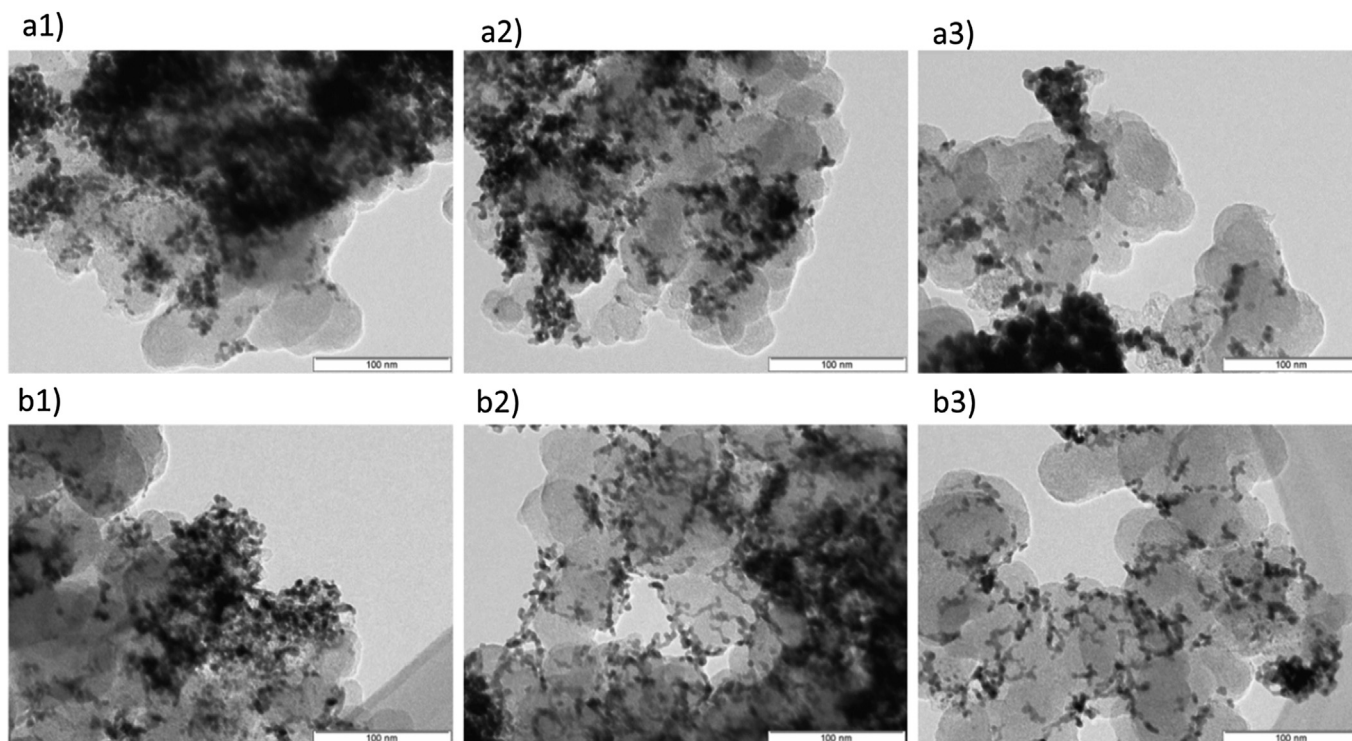

Fig. 10. TEM micrographs representative of anode material after durability testing: a) PtRu/C, and b) PtRu/C–N2. b1 and b2 demonstrate morphology similar to the undoped catalyst. b3 shows areas with different type of catalyst morphology than in the undoped catalyst.

MEAs start with no Ru (Pt-only), Ru crossover from the anode to the cathode occurs even at what is considered 0 h of MEA testing, likely due to the fuel cell break-in protocol. Supplementary Fig. 2 compares the 0 h and 425 h cathode CO stripping curves of both MEAs. At 0 h, the MEA made with the post-doped anode exhibits more Ru crossover than its unmodified counterpart. This is similar to what was found during testing of anodes made with PtRu on pre-doped supports [36]. After 425 h of durability testing, the apparent amount of Ru crossover substantially increases for both MEAs, with the MEA made with post-doped PtRu/C (PtRu/C—N2) having a slightly higher and narrower Pt peak than the MEA made with the unmodified PtRu/C. This is also similar to what was found with pre-doped materials under long term (>400 h) durability testing [36].

3.4. Post-mortem TEM analysis

Fig. 10 shows TEM micrographs that were obtained from the powder extracted from the anode side of both MEAs after 425 h of durability testing. Similar to the materials before durability testing, the powders evaluated after MEA testing also had a large fraction of PtRu in agglomerations (Fig. 10 a1 and b1). Despite the limitations in using TEM to analyze metal nanoparticles supported on carbon particles, overall inspection of the both anode catalysts after durability testing does indicate that both materials lost significant amount of PtRu with a clear loss in particle density accompanied by particle coarsening/agglomeration (Fig. 10 a2, a3, b2 and b3). Analysis of less agglomerated regions, however, suggests that the surface coverage and distribution of nanoparticles on the surface are distinctively different on the unmodified and post-modified anode catalysts. Significantly, analysis of PtRu/C—N2 reveals that some fraction of nanoparticles appear to have strong interaction with surface, apparent from the formation of worm-like nanoparticles covering the carbon surface (Fig. 1 b2 and b3). The worm-like morphology suggests that the post-doped material has additional carbon—support interaction that the undoped material does not have. These observations directly support the electrochemical surface area observations (from the anode CO stripping experiments) that the post-modified anode catalyst material has higher surface areas than its unmodified counterpart. It is likely that higher active surface area of the post-modified anode catalyst observed after 425 h of durability results from the stronger catalyst—substrates interactions due to nitrogen defects that mitigate catalyst migration and coalescence.

4. Conlusions

The results of this work show that after durability testing, the performance of the post-doped commercial anode surpasses that of the undoped commercial anode catalyst. These results are similar to those observed with the *in-house* synthesized catalysts that were pre-doped (i.e., their supports were modified with nitrogen prior to metal deposition) [36]. For the pre-doped catalysts, the greatest improvement in durability was attributed to reduced catalyst migration and coalescence on the nitrogen-modified support. These pre-doped materials included nitrogen in the carbon structure underneath and around the nanoparticles themselves. In the post-modified sample, nitrogen heteroatoms are expected to incorporate only into the carbon regions that are unshielded by nanoparticles without altering the carbon structure directly under the nanoparticles themselves (due to shadowing during implantation). Nevertheless, this post-metal nitrogen-modification process also appears to be effective in improving durability. A density functional theory (DFT) study on Pt interactions with nitrogen-doped highly oriented pyrolytic graphite (HOPG) showed that most nitrogen defects in carbon are negatively charged, attracting

electron density and making the surrounding nearest-neighbor carbon atoms more positive. It was suggested that these nearest neighbor carbons have attractive interactions with Pt and therefore likely restrict Pt migration. Since nitrogen acts as a negative defect it actually repels Pt [13,33], making it seems reasonable to assume that it is energetically unfavorable for Pt to migrate over nitrogen defects. Thus nitrogen-doping, whether it is performed before or after metal deposition, has the potential to create traps for metal particles by making areas where it is unfavorable for the metal to migrate (the nitrogen defects) [56]. This also creates adjacent sites (the more positively charged nearest neighbor carbons) where it is more energetically favorable for the metal to adsorb.

In this work we have shown that nitrogen implantation re-organizes the PtRu composition and its spatial distribution on the surface, which results in a higher density of active sites. Durability testing revealed the initial improvement in surface area and performance was maintainable even after hundreds of hours of operation, highlighting the effectiveness of this technique for commercial applications. In summary, the effects of nitrogen modification on the performance of supported Pt based electrocatalysts after electrochemical durability testing are observed for materials where 1. Nitrogen is introduced before preferential metal deposition 2. Nitrogen is introduced before deposition of metal without preference for defect sites 3. Nitrogen is incorporated after metal deposition.

Incorporating nitrogen into the carbon support before adding metal nanoparticles is likely the most efficient way to gain all of the positive effects attributed to nitrogen-doping, including smaller nanoparticles and higher ECSA due to preferential nucleation, [57–61] increased Pt immobilization [62]. increased electrochemical activity [57–60]. and increased durability [13,26,31,63]. However, modifying the carbon support after metal deposition allows for a reduction in the complexity associated with the nitrogen effects. As shown in this work, immediate improvement to already highly optimized benchmark commercial catalyst materials is possible by after-the-fact support modification. These findings have important implications for electrocatalysis and a wide range of other applications utilizing carbon supported catalysts.

Acknowledgments

Appendix A. Supplementary data

Supplementary data related to this article can be found at http://dx.doi.org/10.1016/j.jpowsour.2013.09.067.

References

[1] X. Yu, S. Ye, J. Power Sources 172 (2007) 145–154.
[2] R. Borup, et al., Chem. Rev. 107 (2007) 3904–3951.
[3] J. Yu, T. Matsuura, Y. Yoshikawa, M. Nazrul Islam, M. Hori, Phys. Chem. Chem. Phys. 7 (2005) 373.
[4] A.K. Shukla, J. Electrochem. Soc. 141 (1994) 1517.
[5] Z. Lei, et al., Microporous Mesoporous Mater. 119 (2009) 30–38.
[6] X. Li, S. Park, B.N. Popov, J. Power Sources 195 (2010) 445–452.
[7] S. Maldonado, K.J. Stevenson, J. Phys. Chem. B 109 (2005) 4707–4716.
[8] N.L. Pocard, D.C. Alsmeyer, R.L. McCreery, T.X. Neenan, M.R. Callstrom, J. Mater. Chem. 2 (1992) 771–784.

[9] K. Prehn, A. Warburg, T. Schilling, M. Bron, K. Schulte, Compos. Sci. Technol. 69 (2009) 1570–1579.
[10] M. Terrones, et al., Adv. Mater. 11 (1999) 655–658.
[11] G. Vijayaraghavan, K.J. Stevenson, Langmuir: ACS J. Surf. Colloids 23 (2007) 5279–5282.
[12] C. Sun, et al., Chem. Mater. 17 (2005) 3749–3753.
[13] Y. Zhou, et al., Energy Environ. Sci. 3 (2010) 1437.
[14] S. Maldonado, S. Morin, K.J. Stevenson, Carbon 44 (2006) 1429–1437.
[15] U. Bangert, A. Bleloch, M. Gass, A. Seepujak, J. van den Berg, Phys. Rev. B 81 (2010) 1–11.
[16] V.V. Strelko, V.S. Kuts, P.A. Thrower, Carbon 38 (2000) 1499–1503.
[17] S.C. Roy, J. Electrochem. Soc. 143 (1996) 3073.
[18] K.N. Wood, et al., ACS Appl. Mater. Interfaces 4 (2012) 6728–6734.
[19] L.C. Chen, et al., Adv. Funct. Mater. 12 (2002) 687–692.
[20] Y. Chen, et al., Electrochem. Commun. 11 (2009) 2071–2076.
[21] S. Ye, J. Electrochem. Soc. 144 (1997) 90.
[22] T. Maiyalagan, B. Viswanathan, U.V. Varadaraju, Electrochem. Commun. 7 (2005) 905–912.
[23] K.N. Wood, et al., MRS Commun. 2 (2012) 85–89.
[24] T. Maiyalagan, Appl. Catal. B Environ. 80 (2008) 286–295.
[25] G. Wu, D. Li, C. Dai, D. Wang, N. Li, Langmuir: ACS J. Surf. Colloids 24 (2008) 3566–3575.
[26] S. Pylypenko, et al., J. Phys. Chem. C 115 (2011) 13676–13684.
[27] S. Pylypenko, et al., J. Phys. Chem. C 115 (2011) 13667–13675.
[28] Y. Zhou, et al., J. Mater. Chem. 19 (2009) 7830.
[29] S. Ye, J. Electrochem. Soc. 143 (1996) L7.
[30] G. Liu, X. Li, P. Ganesan, B.N. Popov, Appl. Catal. B Environ. 93 (2009) 156–165.
[31] Y. Shao, J. Sui, G. Yin, Y. Gao, Appl. Catal. B Environ. 79 (2008) 89–99.
[32] T. Kondo, T. Suzuki, J. Nakamura, J. Phys. Chem. Lett. 2 (2011) 577–580.
[33] S. Pylypenko, et al., in: 220th ECS Meeting, 2011.
[34] S. Pylypenko, et al., in: Abstracts of Papers of the American Chemical Society, vol. 242, 2011.
[35] P. Joghee, et al., J. Electrochem. Soc. 159 (2012) F768–F778.
[36] A.R. Corpuz, et al., J. Power Sources 217 (2012) 142–151.
[37] A.A. Dameron, et al., ACS Catal. 1 (2011) 1307–1315.
[38] T.S. Olson, et al., J. Electrochem. Soc. 160 (2013) F389–F394.
[39] K.M. McGrath, G.K.S. Prakash, G.A. Olah, J. Ind. Eng. Chem. 10 (2004) 1063–1080.
[40] M. Baldauf, W. Preidel, J. Power Sources 84 (1999) 161–166.
[41] S. Sharma, B.G. Pollet, J. Power Sources 208 (2012) 96–119.
[42] H.N. Dinh, X. Ren, F.H. Garzon, S. Gottesfeld, J. Electroanal. Chem. 491 (2000) 222–233.
[43] S. Pylypenko, et al., in: Preprints of Papers – American Chemical Society, Division of Fuel Chemistry vol. 56, 2011, pp. 264–265.
[44] I. Kusunoki, et al., Surf. Sci. 492 (2001) 315–328.
[45] K. Artyushkova, S. Pylypenko, T.S. Olson, J.E. Fulghum, P. Atanassov, Langmuir: ACS J. Surf. Colloids 24 (2008) 9082–9088.
[46] F. Jaouen, et al., ACS Appl. Mater. Interfaces 1 (2009) 1623–1639.
[47] S. Pylypenko, S. Mukherjee, T.S. Olson, P. Atanassov, Electrochim. Acta 53 (2008) 7875–7883.
[48] T.S. Olson, et al., J. Phys. Chem. C 114 (2010) 5049–5059.
[49] S. Pylypenko, et al., ECS Transactions, vol. 33, The Electrochemical Society, 2010, pp. 351–357.
[50] H.A. Gasteiger, N. Markovic, P.N. Ross, E.J. Cairns, J. Phys. Chem 98 (1994) 617–625.
[51] M. Watanabe, M. Uchida, S. Motoo, J. Electroanal. Chem. Interfacial Electrochem. 229 (1987) 395–406.
[52] D. Chu, J. Electrochem. Soc. 143 (1996) 1685.
[53] Z. Liu, X.Y. Ling, X. Su, J.Y. Lee, J. Phys. Chem. B 108 (2004) 8234–8240.
[54] R. Dillon, S. Srinivasan, A.S. Aricò, V. Antonucci, J. Power Sources 127 (2004) 112–126.
[55] W. Li, et al., J. Phys. Chem. B 107 (2003) 6292–6299.
[56] C.L. Muhich, J.Y. Westcott, T.C. Morris, A.W. Weimer, C.B. Musgrave, J. Phys. Chem. C (2013), 130422101110001.
[57] S.C. Roy, J. Electrochem. Soc. 144 (1997) 2323.
[58] S.-H. Liu, et al., J. Mater. Chem. 21 (2011) 12489.
[59] Y. Chen, et al., J. Phys. Chem. C 115 (2011) 3769–3776.
[60] D.C. Higgins, D. Meza, Z. Chen, J. Phys. Chem. C 114 (2010) 21982–21988.
[61] Z. Lei, et al., J. Mater. Chem. 19 (2009) 5985.
[62] B. Yue, et al., J. Mater. Chem. 18 (2008) 1747.
[63] Z. Liu, F. Su, X. Zhang, S.W. Tay, ACS Appl. Mater. Interfaces 3 (2011) 3824–3830.